Highly sensitive and selective acute myocardial infarction detection using aptamer-tethered MoS_2 nanoflower and screen-printed electrodes

Mugashini Vasudevan[1,2]
Melvin J.Y. Tai[1,2]
Veeradasan Perumal[1,2*]
Subash C.B. Gopinath[3,4]
Satisvar Sundera Murthe[1,5]
Mark Ovinis[2]
Norani Muti Mohamed[1,5]
Nirav Joshi[6,7]

[1]*Centre of Innovative Nanostructures and Nanodevices (COINN), Universiti Teknologi PETRONAS, Seri Iskandar, Perak Darul Ridzuan, Malaysia*

[2]*Department of Mechanical Engineering, Universiti Teknologi PETRONAS, Seri Iskandar, Perak Darul Ridzuan, Malaysia*

[3]*Institute of Nano Electronic Engineer, Universiti Malaysia Perlis, Kangar, Perlis, Malaysia*

[4]*School of Bioprocess Engineering, Universiti Malaysia Perlis, Arau, Perlis, Malaysia*

[5]*Department of Fundamental and Applied Sciences, Universiti Teknologi PETRONAS, Seri Iskandar, Perak Darul Ridzuan, Malaysia*

[6]*Sao Carlos Institute of PhysicsUniversity of Sao Paulo, Sao Carlos, Sao Paulo, Brazil*

[7]*Department of Mechanical Engineering, University of California, Berkeley, CA, USA*

Abstract

Acute myocardial infarction (AMI) is one of the leading causes of death worldwide. Cardiac troponin I (cTn1) is a commonly used biomarker for the diagnosis of AMI. Although there are various detection methods for the rapid detection of cTn1 such as optical, electrochemical, and acoustic techniques, electrochemical aptasensing techniques are commonly used because of their ease of handling, portability, and compactness. In this study, an electrochemical cTn1 biosensor, MoS_2 nanoflowers on screen-printed electrodes assisted by aptamer, was synthesized using hydrothermal technique. Field emission scanning electron microscopy revealed distinct 2D nanosheets and jagged flower-like 3D MoS_2 nanoflower structure, with X-ray diffraction analysis revealing well-stacked MoS_2 layers. Voltammetry aptasensing of cTn1 ranges from 10 fM to 1 nM, with a detection limit at 10 fM and a sensitivity of 0.10 nA μM^{-1} cm^{-2}. This is a ~fivefold improvement in selectivity compared with the other proteins and human serum. This novel aptasensor retained 90% of its biosensing activity after 6 weeks with a 4.3% RSD and is a promising high-performance biosensor for detecting cTn1. Volume 0, Number 0, Pages 1–10, 2020

Keywords: *acute myocardial infarction, aptasensor, biomarker, molybdenum disulfide, troponin I*

Abbreviations: *AC, alternating current; Ag, silver; AMI, acute myocardial infarction; APTES, (3-Aminopropyl) triethoxysilane; CM, complex mixture; DMF, N,N-Dimethylformamide; ECG, electrocardiogram; EDC, carbodiimide hydrochloric; EIS, electrochemical impedance spectroscopy; ELISA, enzyme-linked immunosorbent assay; FESEM, field emission scanning electron microscopy; FT-IR, Fourier transform infrared spectroscopy; LOD, limit of detection; Mo, molybdenum; MoS_2, molybdenum disulfide; NFs, nanoflowers; NHS, N-hydroxysuccinimide; NS, nanosheets; PBS, phosphate buffer saline; Rct, charge transfer resistances; RSD, relative standard deviation; S, sulphur; 2D, two dimensional; 3D, three dimensional; SPE, screen printed electrode; STPVD, streptavidin; TEM, transmission electron microscopy; XPS, X-rat photoelectron spectroscopy; XRD, X-ray diffraction.*

**Address for correspondence: Veeradasan Perumal, Centre of Innovative Nanostructures and Nanodevices (COINN), Universiti Teknologi PETRONAS, 32610 Seri Iskandar, Perak Darul Ridzuan, Malaysia. Tel.: +60 10 3773747; e-mail: veeradasan.perumal@utp.edu.my.*

Additional supporting information may be found online in the Supporting Information section at the end of the article.

1. Introduction

Acute myocardial infarction (AMI) or a heart attack is a life-threatening condition with an alarming mortality rate [1]. AMI disrupts blood flow to the heart, causing irreversible tissue damage [2]. Clinical methods used to diagnose AMI such as electrocardiogram, stress test, angiogram, and echocardiogram are time consuming with long waiting lists, which are problematic as [3] patients with AMI require early treatment for better prognosis. A common solution is the use of blood-based biomarkers.

Biomarkers are natural proteins that can be used to detect the presence of a disease. Most diseases have a unique set of biomarkers and altered levels of these markers is indicative of a disease. Examples of cardiac biomarkers are myoglobin, creatine-kinase MB, C-reactive protein, and cardiac troponin [4]. Since the 1980s, troponin I has been the "gold standard" biomarker to detect AMI [5,6]. Troponin I is released into the blood stream when heart tissue is damaged during a heart attack. AMI biomarkers have been identified using electrochemical and optical methods such as surface plamon resonance [7], chemiluminescence, aptasensor, fluorescence, colorimetric, enzyme-linked immunosorbent assay, and immunosensors [8].

In particular, aptamer-based electrochemical method or aptasensor is a quick and effective way to detect biomarkers with high sensitivity and selectivity [9]. Aptamers are artificial nucleic acid ligands that have high binding efficiency and are mostly used in clinical-based biosensors to detect desired pathogen of infectious diseases with high selectivity [10]. A nanomaterial such as molybdenum disulfide (MoS_2) can increase the sensitivity of the electrochemical interactions of aptamer and troponin I by enhancing its surface area. MoS_2 is a transition metal disulfide with a large surface area, rich surface chemistry, and excellent biocompatibility.

In this work, we have successfully developed 2D-MoS_2 nanosheets (NSs) and 3D-flower-like MoS_2 through the finely tuned hydrothermal method as this method can lead to two different MoS_2 structure. The morphological, structural, and optical properties was analyzed and compared between 2D-MoS_2 NSs and 3D-flower-like MoS_2 to determine its capability as active material in biosensing application. 3D-flower-like MoS_2 nanoflowers (MoS_2 NFs) have enhanced biomarker detection owing to the wider surface area provided by the NFs, leading to higher biomolecular attachments. In addition, MoS_2 NFs have rapid electron transfer because of lower impedance, as measured through impedance spectroscopy analysis. This novel fabricated biosensor can detect troponin I in human serum at low concentrations with high degree of selectivity despite the presence of other biomarkers and biological ligands [4] and it also has excellent potential to be utilized for the detection of CnT1.

Highlights

- Fabricated MoS_2 nanostructures in 2D & 3D dimensions under hydrothermal method
- 3D- nanoflower on aptamer-tethered screen printed triple electrodes was explored
- Limit of detection (LOD) was up to 10 fM for cardiac biomarker Troponin I detection
- Validation with human serum shown the greatest potential with similar sensitivity
- High-performance was proved with selectivity, reproducibility and stability

2. Materials and Methods

2.1. Chemicals and materials

The initial materials utilized are molybdenum (VI) oxide, 16-mercaptohexadecanoic acid 99%, 1-ethyl-3-(3-dimethylaminopropyl)carbodiimide (EDC), silver nanoparticles (AgNPs), N-hydroxysuccinimide (NHS), streptavidin (STVD), 1× phosphate-buffered saline (PBS), and (3-aminopropyl) triethoxysilane (APTES) were all obtained from Sigma–Aldrich Co. (USA). Ammonium heptamolybdate tetrahydrate, L-cysteine, thiourea, hydrochloric acid (37%), ethanolamine, and ethanol absolute were obtained from Merck & Co. (USA). All of the chemicals were utilized as received without any extra purification steps. The oligonucleotides were purchased from Avantis Laboratory (USA). The details of the oligonucleotide sequences utilized in this current work were as follows:

Probe (Aptamer): 5′-CGT GCA GTA CGC CAA CCT TTC TCA TGC GCT GCC CCT CTT AAA AAA AAA AAA AAA AAA AAA AAA A-3′; Biotin oligo linker: 5′-/5Biosg//iC6Sp/TTT TTT TTT TTT TTT TT-3′; Target: Troponin I; Control: Troponin T; Human Serum from human male AB plasma purchased from Sigma–Aldrich Co. (Malaysia).

Commercialized transducer screen-printed electrode (SPE) was purchased from Metrohm DropSens (Malaysia).

2.2. Fabrication of MoS_2 NFs and MoS_2 NSs

MoS_2 NFs and MoS_2 NSs were synthesized based on the methods by Zhu et al. [11] and Veeramalai et al.[12]. A detailed description on the synthesis method of MoS_2 NFs and MoS_2 NS is shown in the Supplementary Information. A black precipitate was obtained after hydrothermal treatment was washed three times using absolute ethanol followed by distilled water. Both MoS_2 products were then transferred into a 30 mL crucible and dried. MoS_2 NFs were dried at 60 °C for 12 H, whereas MoS_2 NS was dried overnight at 45 °C in an oven. Next, the completely

Received 8 August 2020; accepted 21 October 2020
DOI: 10.1002/bab.2060
Published online in Wiley Online Library (wileyonlinelibrary.com)

dried MoS_2 NFs and MoS_2 NSs were placed inside a desiccator for storage purposes.

2.3. Microscopic-nanoscale imaging

The surface morphology of the of MoS_2 NFs and MoS_2 NSs was characterized by variable pressure field emission scanning electron microscopy (VP-FESEM) (Carl Zeiss SUPRA55 VP; Gemini). The nanoscale imaging was investigated using transmission electron microscopy (TEM). High-resolution TEM (HRTEM) images of MoS_2 NFs were carried out using a HITACHI HT 7830 series up to 120 kV. Sample preparation was carried out by dispersing MoS_2 NFs in double distilled water and sonicated for 10 Min before dropping the sample on TEM grid.

2.4. Structural analysis and optical measurements

Powder X-ray diffraction (XRD) was conducted using X'Pert^3 Powder & Empyrean, PANalytical.with a Cu Kα radiation ($\lambda = 1.54$ Å) was used to study the crystallization and structural properties of MoS_2 NFs and MoS_2 NSs . The XRD pattern was recorded in the range of 10°–80° operating at a voltage of 40 kV and a current of 30 mA. The immorbilization, interaction, and material composition were analyzed using XPS (Thermo Scientific K-Alpha). Fourier transform infrared spectroscopy (FT-IR) (Brand: PerkinElmer Inc.; Spectrum One/BX) were used to identify the functional groups exist in the prepared materials. The wave range is from 7,800 to 350 cm^{-1} at resolution from 0.5 cm cm^{-1} to 64 cm^{-1}.

2.5. Impedance spectroscopy

Electrical measurements of current to voltage (*I–V*) were carried out using (Kiethley 6487 Picoammeter) as the voltage source set from 0 to 2 V, with two wired point-probing to characterize the di-electrode system on SPE surface. Electrochemical impedance spectroscopy (EIS) measurements were performed with Metrohm Multi Autolab M204 Potentiostat/Galvanostat. All the measurements were done at room temperature.

2.6. Surface functionalization on SPE

Commercially available SPEs were prepared for surface modifications. The *I–V* reading for each electrode was measured with the addition of 10 µL of 10 mM PBS with a pH of 7.4 to check for fabrication error and to test the repeatability of the bare SPE chips. 2% of APTES was then dropped on the surface bare SPE chip and left to incubate at room temperature for an hour. The chip was subsequently washed twice using 10 mM PBS with a pH of 7.4 to remove any remaining APTES that was not immobilized on the surface of the electrode. The *I–V* reading for the electrode immobilized with 2% APTES was taken. The pellet obtained after centrifugation of complex mixture (CM) was taken and dropped onto the APTES-modified surface of the SPE electrode. CM was used to reduce the number of surface modification steps instead of doing one-by-one (layer-by-layer). The CM consists of 16-mercaptohexadecanoic acid together with NHS, carbodiimide hydrochloride, and AgNPs. Addition of AgNPs enhances the surface area with ultimate capturing of molecules and also induces the analytical performance of the developed sensor, which significantly gives higher sensitivity of the device. To prepare this mixture, 16-mercaptohexadecanoic acid powder was measured and diluted in 50% ethanol. Fifty microliters of diluted 16-mercaptohexadecanoic acid was then mixed with 25 µL of 200 mM EDC, 25 µL of 50 mM NHS, and 1 mg/mL of AgNPs. The mixture was left to interact for 10 Min and centrifuged for 2 Min at 10,000×*g*. The electrode was then left for 15 Min at room temperature. Next, the modified surface CM/APTES/SPE was washed by PBS and measured. Electrical Impedance spectroscopy measurements were taken for MoS_2 NFs and MoS_2 NSs to determine their impedance values before proceeding with surface modification of the electrode with MoS_2 NFs. NHS and EDC were then used to enhance and activate the SPE electrode. 1 mg/mL of MoS_2 NFs powder (hydrothermal method) was dropped on the CM/APTES/SPE and incubated for 30 Min. The modified electrode was then washed and the measurement for MoS_2_NF/CM/APTES /SPE was obtained. Furthermore, layer-by-layer surface modification of APTES and CM on SPE was to provide good binding affinity for MoS_2. Ten microliters of STVD (50 µL of 200 nM STVD was then mixed with 25 µL of 200 mM EDC and 25 µL of 50 mM NHS), dropped on the MoS_2_NF/CM/Aptes/SPE and incubated for 30 Min. After that, the modified electrode was washed, and *I–V* reading was taken. Ethanolamine (ETNE) (1 M), which acts as a blocking agent, was dropped on the surface of the STVD/MoS_2_NF/CM/APTES/SPE to block the areas that were not immobilized on the surface of the STVD/MoS_2_NF/CM/APTES/SPE. The incubation process was carried out for 30 Min. After that, the modified ETNE/STVD/MoS_2 NF/CM/APTES/SPE electrode was washed and *I–V* reading was taken.

2.7. Immobilization and interaction of target

The dilution of the probe before immobilizing it on the surface of modified SPE is shown in the Supplementary Information. After diluting the probe, 1 µM of the probe was dropped on the modified surface of ETNE/STVD/MoS_2_NF/CM/Aptes/SPE to obtain the aptamer-conjugated ETNE/STVD/MoS_2_NF/CM/Aptes/SPE electrode. The aptamer–biotarget interaction was carried out by diluting the target (troponin I) with different concentrations ranging from 10 fM to 1 nM in 10 mM PBS of pH 7.4 at room temperature. The hybridized troponin I/aptamer/ETNE/STVD/MoS_2_NF/CM/Aptes/SPE electrode was then washed with 10 mM PBS of pH 7.4 and the impedance spectroscopy measurement was taken for each concentration to determine the detection limit of troponin I using the chemically modified electrode. This was repeated using different concentrations of biotarget and different dilutions of human serum. A detailed schematic illustration for immobilization and interaction of troponin I biosensor is shown in Fig. 1 and Fig. S1.

2.8. Detection of troponin I in human serum

The detection of troponin I in human serum was conducted by diluting 1 µL of pure human serum with 10 mL of 10 mM PBS of pH 7.4 to obtain a dilution factor of 1:10,000. A 1:10,000

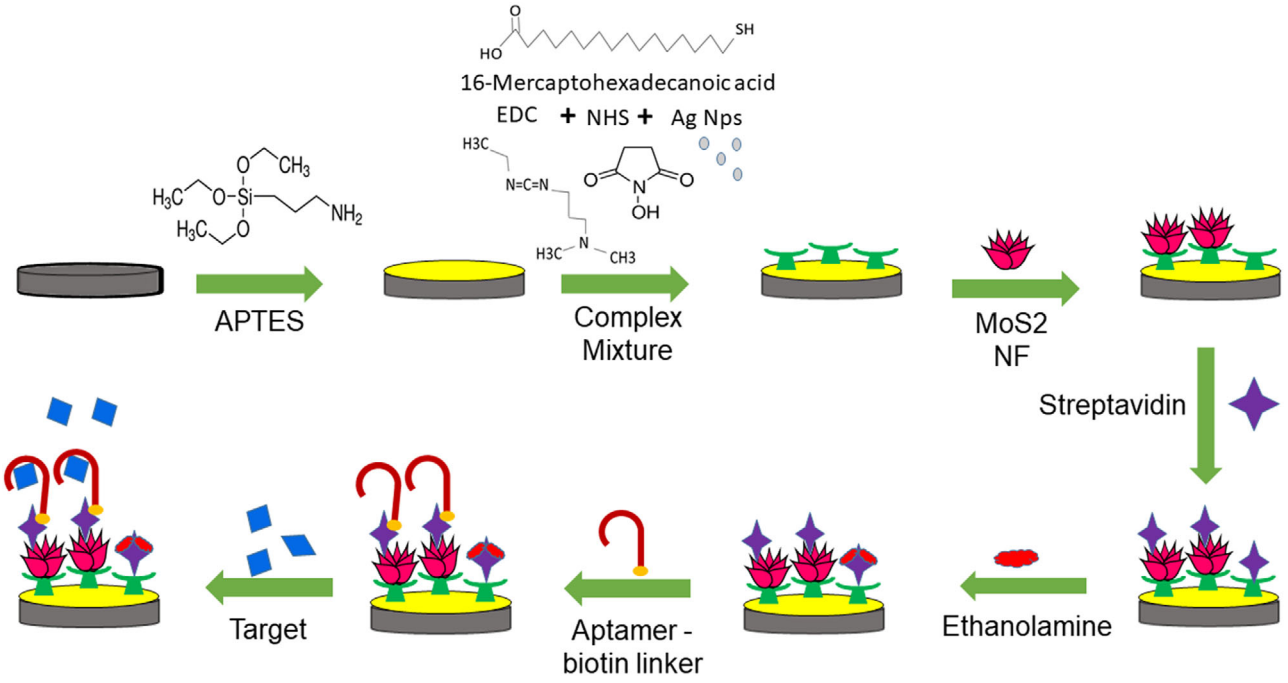

FIG. 1 *Detailed schematic illustration of the steps involved in surface modification, immobilization, and interaction to recognize acute myocardial infarction biomarker.*

dilution factor was used as a buffer solution to dilute the biotarget at different concentrations (10 fM to 1 nM) to form troponin I spiked sample similar to the method described in Section 2.4 for target concentration dilution. In that regard, the human serum was diluted from 1:10 to 1:10,000 using 10 mM PBS at pH 7.4. These different dilutions factors in human serum were analyzed through the voltammetry analyses to test the ability of the aptamer-modified MoS_2 NFs electrode to identify and select the target as the concentration of target in human serum decreases as the dilution increases as shown in Fig. S2. The rest of the surface chemical modifications and detection strategies employed were identical.

2.9. Stability and repeatability analysis

Stability of the hybridized electrode was checked on a weekly basis by applying 10 µL of PBS on the surface of the electrode and measuring its impedance. The stability test was done for every electrode that was used for target detection and human serum detection. As for the repeatability, the impedance measurements taken were repeated using different SPE electrodes to ensure that every electrode gave approximately similar readings for similar materials.

3. Results and Discussion

Electrochemical impedance spectroscopy is effective for precisely measuring the charge transfer processes within electrochemical sensors [13,14]. EIS analysis was carried out to quantify the electrochemistry of MoS_2 NFs and MoS_2 NSs before being immobilized and hybridized on the SPE electrode. The EIS data were fitted to a Randles equivalent circuit to determine the charge transfer resistance (Rct) value. The corresponding Nyquist plot is shown in Fig. S3 in the Supplementary Information, where the interfacial charge transfer resistance of MoS_2 NF is smaller than the interfacial charge transfer resistance of MoS_2 NSs. The Rct value of MoS_2 NF is 0.28 MΩ, whereas Rct value of MoS_2 NS is 0.64 MΩ. High Rct value shows that the current flow was impeded. This results in very low electrical conductivity and leads to a slower transfer of electrons. On the other hand, low Rct value implies that MoS_2 NFs have better capacitive behavior with lower diffusion resistance of ions. The differences in the electrochemical signal of MoS_2 material are due to disparity in the material–electrolyte interface properties and the electrolyte ion diffusion rates during the charge–discharge processes. Impedance spectroscopy measurement shows that MoS_2 NFs have lower impedance compared with the MoS_2 NSs. MoS_2 NFs therefore have higher electrical conductivity, with greater number of active sites due to its three-dimensional morphology compared with the MoS_2 NSs. MoS_2 NFs were therefore used for immobilization and interaction, as it will provide greater sensitivity and selectivity for troponin I detection.

3.1. Field-emission scanning electron microscopy

MoS_2 has a sheet form due to its intrinsic lamellar structures. These sheets clump together during the hydrothermal treatment due to Van der Waals interaction and self-assemble into three-dimensional nanostructure to form NFs [15, 16]. Figures 2A and 2B show the FESEM image of MoS_2 NSs. The NSs are not uniformly arranged and have different vertical sizes [17]. They have wave-like morphology with some areas densely

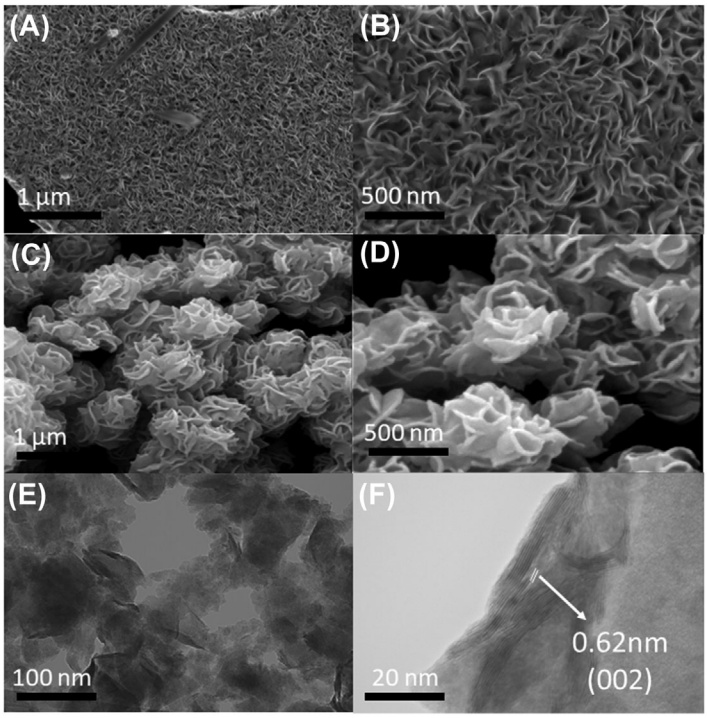

FIG. 2 *FESEM image of MoS_2 nanostructure. (A) Low and (B) high magnifications image of MoS_2 nanosheet and (C) low and (D) high magnification of MoS_2 nanoflower are shown. The scanning electron microscope uses a focused beam of high-energy electrons up to 30 kV. (E) A typical TEM image of MoS_2 nanoflower at 100 nm. (F) A high-resolution TEM image of the lattice fringes of MoS_2 nanoflower layers.*

packed to form a rough surface. The NSs were combined in a single plane resulting in a two-dimensional MoS_2 NS structure. In Figs. 2C and 2D, it can be observed that each NF is distinct and have similar flower structure, with MoS_2 NFs having a larger surface area then MoS_2 NS. Wider structure (large surface area) that attributes to high number of active sites of MoS_2 NFs improves the sensitivity of MoS_2 NFs-based sensor by increasing the chances of immobilization and interaction of the probe and biotarget. In short, MoS_2 NFs are the best morphological structure to be used as active material in biosensing application.

3.2. Transmission electron microscopy

Figures 2E and 2F show TEM images at both low and high magnifications. Figure 2E shows that MoS_2 NFs are interconnected, forming a three-dimensional NF structure [18]. MoS_2 NFs accrue at certain areas, which made those regions denser than other regions. The MoS_2 layers are interconnected due to Van der walls interaction between layers [12]. The top view of the HRTEM image shown in Fig. 2F shows that the MoS_2 NF consists of a few layers with each petal consisting of 4–7 MoS_2 layers with an interlayer spacing of 0.62 nm, corresponding to the (0 0 2) plane of MoS_2, as indicated by XRD results [19,20]. The interlayer spacing of 0.62 nm and (0 0 2) plane in XRD shows a well-defined crystal structure formed in MoS_2 NFs [18,21].

3.3. X-ray photoelectron spectroscopy

X-ray photoelectron spectroscopy (XPS) studies were conducted to determine the chemical state, the composition and energy of electrons emitted from the surface of aptamer/ETNE/STVD/MoS_2_NF/CM/Aptes/SPE. In Fig. 3A, a wide XPS survey scan shows the presence of carbon, nitrogen, oxygen, phosphorus, sulfur, and molybdenum. The C 1s spectrum in Fig. 3B with binding energies of 286.2 and 289.4 eV corresponds to C–O–C and C–O bonds [22,23]. The peaks related to O 1s at 531.7 eV can be attributed to impurities in the fabricated sample [12], as shown in Fig. 3C. The N1 s spectrum in Fig. 3D indicates the presence of two peaks at 399.8 and 402.6 eV, whereas the P 2p spectrum in Fig. 3E indicates the existence of binding energy at 133.8 eV. Further, in Fig. 3F, two noticeable high-resolution core level spectrum Mo 3d peaks can be observed at 231.4 and 234.5 eV, which corresponds to Mo $3d_{5/2}$ and Mo $3d_{3/2}$, indicating the formation of Mo^{4+} oxidation state, where MoS_2 layers were formed [24]. As for the peaks for S 2p shown in Fig. 3G, the observed binding energy of 164 and 168.3 eV can be attributed to S $2p_{3/2}$ and S $2p_{1/2}$, respectively [19,25]. These data confirm the structure and composition of MoS_2 NFs.

3.4. X-ray diffraction

X-ray diffraction measurements were carried out to identify the crystal structure of the fabricated materials. The MoS_2 NFs and MoS_2 NSs have crystalline structures at different degrees, as shown in Fig. 4. In Fig. 4A, the diffraction peaks for MoS_2 NFs corresponds to a well-defined hexagonal structure, with diffraction peaks at 14.0°, 33.5°, 40.1° 49.35°, and 58.9°, corresponding to the (0 0 2), (1 0 0), (1 0 3), (1 0 5), and (1 1 0) planes of MoS_2 [19]. The broadening of (1 0 3) and (1 0 5) and the shift of (0 0 2) peak are consistent with the formation of the defects in the nanosized flower. Besides that, MoS_2 NFs have a (0 0 2) diffraction peak, which indicates a well-stacked layer of MoS_2. No other peak has been observed in the XRD pattern, indicating the synthesized MoS_2 NFs has no impurities. As for MoS_2 NS in Fig. 4B, the absence of (0 0 2) plane indicates that the stacking of the (0 0 2) plane in the 2D MoS_2 NSs is significantly inhibited and an extremely thin NSs was obtained [26]. The diffraction peaks for MoS_2 NS were at 26.1°, 32.8°, 36.9°, 53.5°, 60.6°, 66.9°, 72.9°, and 79.5°, which corresponds to T(11-1), TR(10-2), T(200), T(31-1), M(130), TM(021), M(311), and TM(040). After riveted refinement, the percentage of molybdenite forms in MoS_2 NFs is 96.3 wt%, whereas the percentage of rosickyite low is 3.7 wt%. On the other hand, the percentage of molybdenum dioxide is 30.1 wt%, molybdenite is 43.6 wt%, and sulfur is 26.3 wt% for MoS_2 NS. MoO_3 powder was initially used to fabricate MoS_2 NS but due to the long hydrothermal time, MoO_3 was reduced under the

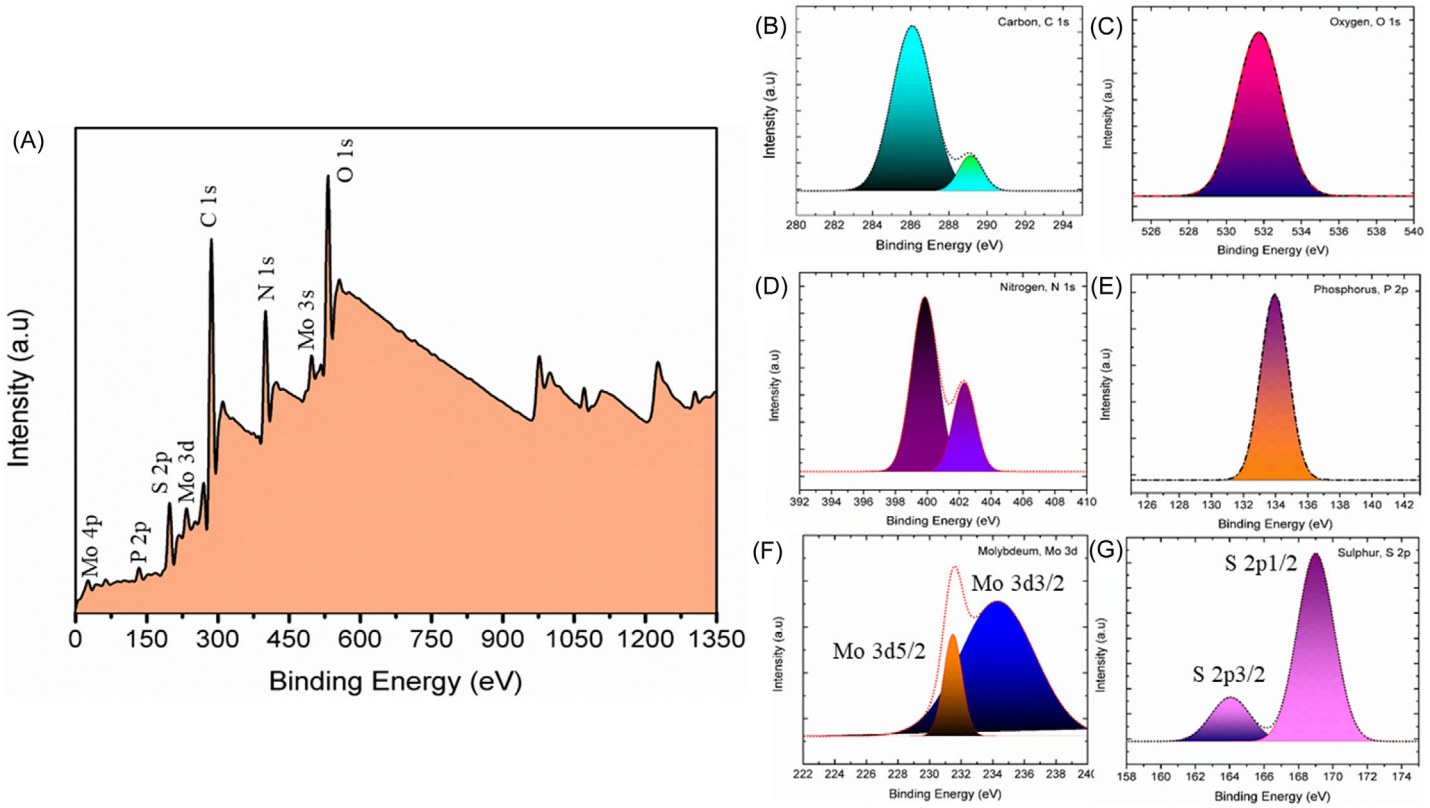

FIG. 3 *(A) Survey scan of XPS core level spectra taken on MoS_2 nanoflower. (B) Binding energy of C, C1s; (C) O, O1s; (D) N, N1s; (E) P, P2p; (F) Mo, Mo3d; (G) S, S2p electrons.*

reducing environment to sub-oxide MoO_2. MoO_2 then reacted with sulfur (L-cysteine) to form MoS_2 [27,28]. It can be seen that the temperature and the time used for the fabrication of MoS_2 affect the formation of crystalline structure [27]. Thus, the existences of (0 0 2) peak obtained from XRD analysis indicates that MoS_2 NFs have well-defined hexagonal structure and well-stacked layer of MoS_2, whereas the absence of (0 0 2) peak of MoS_2 NSs correspond to severe stacking (congested) with thin layers of MoS_2 in which expected to limit the probe–analyte interactions. The result is in good agreement with the FESEM result, which showed MoS_2 NF has a large surface area (3D) with numerous active sites compared with the MoS_2 NS (2D), which efficiently enhances the immobilization and hybridization of probe–analyte.

3.5. FT-IR spectroscopy

FT-IR spectroscopy analysis was conducted to identify the functional groups and bonds present in the fabricated samples. The absorption peaks obtained for MoS_2 NFs and MoS_2 NSs are almost similar as shown in Figs. 4C and 4D. The absorption peaks are visible at 475 and 604.77 cm^{-1} due to Mo–S bonds, whereas Mo–O bond can be seen at 1,100.66 cm^{-1}, corresponding to the stretching vibration of the hydroxyl group and Mo–O vibrations. Furthermore, the S=O stretching bond is prominent in MoS_2 NSs at 1,034.68 cm^{-1}. Other peaks can be seen for both samples at 763.83 cm^{-1} (C–H bending), 903.82 cm^{-1} (C=C bending), 1,118.13 cm^{-1} (C–O stretching), 1,399.91 cm^{-1} (O–H bending), 1,611.78 cm^{-1} (C=C stretching), 2,060.94 cm^{-1} (C–H stretching), 3,119.73 cm^{-1} (O–H stretching), and 3,400.96 cm^{-1} (O–H stretching).

3.6. *I–V* measurement for surface modification on SPE electrode

The electrical signals were measured using a Picoammeter, with two wire point-probing, to determine the changes in the current flow when different materials were added on the SPE before the detection of troponin I. In Fig. 5A, the current value for the bare electrode is the lowest, with a value of 1.9 µA. After APTES was applied on the electrode, the current flow increased to 17 µA, indicating that the amine has interacted at the surface of the SPE electrode. A CM and MoS_2 NFs were then applied for intense modification, where the current flow for each layer modification was 91 and 84 µA, respectively. The current flow of CM was higher than MoS_2 NFs because there was an electrochemical interaction between the CM and MoS_2 NFs. After attaching STVD, the current flow increases to 15 mA and the current flow of ethanolamine increases to 19 mA. To avoid measurement error, ethanolamine was used to block the unreacted site before applying the biotin-linked aptamer. The aptamer consists of biotin linker to interact on the surface of STVD , which enable the current flow of the probe to be higher than STVD , as STVD has four binding sites,

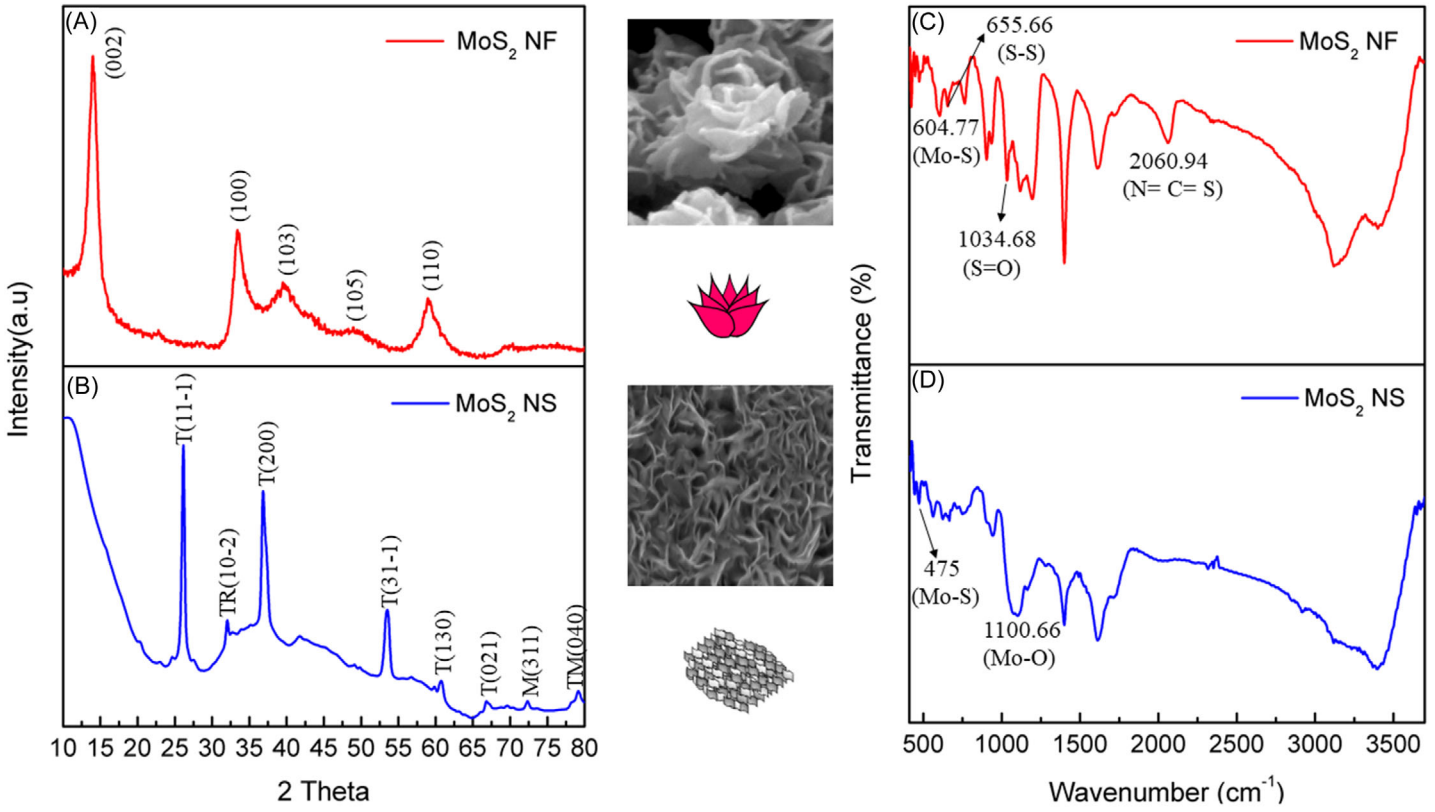

FIG. 4 *XRD image of (A) MoS_2 nanoflower and (B) MoS_2 nanosheet. Showing the semi-crystalline peaks of fabricated nanostructures. FT-IR spectra image of fabricated (C) MoS_2 nanoflower and (D) MoS_2 nanosheet. Absorption regions are shown from 350 to 3,700 cm^{-1}.*

which provide greater interaction opportunities for biotin-linked aptamer. Physical and chemical reaction occurred in every steps of device surface modification to provide a higher binding affinity platform for the probe immobilization, which enhances a large number of immobilization of biotin-linked aptamer on STVD, indicative of a more efficient interaction of target [29–31]. Furthermore in the absence of MoS_2, the resistivity on the SPE surface was highest due to the presence of carbon, which shows non-metal element. Electron flow was disrupted as the interface resistivity was high, which effects the probe–analyte interaction compared with MoS_2 NFs. Since, the resistance is inversely proportional to the current, addition of MoS_2 NF reduces the impedance of the SPE surface and increases the conductivity of the modified surface as MoS_2 NF has semi-conductor properties.

3.7. Determination of limit of detection using *I–V* measurement

Figure 5B illustrates the *I–V* measurement of aptamer-modified SPE electrode at various concentrations of target troponin I (1 nM to 10 fM). The current value at 2 V decreased upon interaction with increasing concentration of target troponin I. 10 fM exhibits high conductivity with low resistance, as evident by the high current value at 8.1×10^{-5} A, compared with the other target concentrations. This is because low charges accumulate less among the target present in 10 fM, allowing aptamer to capture troponin I easily. The highest concentration (1 nM) of troponin I produced a current value of 1.4×10^{-4} A, where high target concentration results in high resistivity. The accumulation of charges caused 1 nM to have low conductivity. As shown in Fig. 5C, at 2 V, there is a slight but significant difference in current from concentrations of 100 pM to 100 fM of target troponin I. The current values for 100 fM to 1 pM concentration of troponin I was 1.3×10^{-4} and 1.0×10^{-4} A, respectively. On the other hand, the current values were 9.4×10^{-5} and 8.4×10^{-5} A for troponin concentrations of 10 and 100 pM, respectively. Therefore, the limit of troponin I detection for this biosensor is 10 fM. A summary of previous studies based on method and strategies used to detect troponin I is shown in Table 1.

3.8. Detection of troponin I in the presence of human serum

Figure 5D shows the impedance analysis of different dilutions of human serum. As the dilution of human serum increases, the Rct increases. The highest Rct level is 4.3×10^5 Ω, which coincides with the highest human serum concentration (1 nM) and the lowest Rct level is 1.6×10^5 Ω, which corresponds to the 10 fM human serum concentration. Human serum with 100 fM and 1 pM corresponds to an Rct of 2.1×10^5 and 2.7×10^5 Ω,

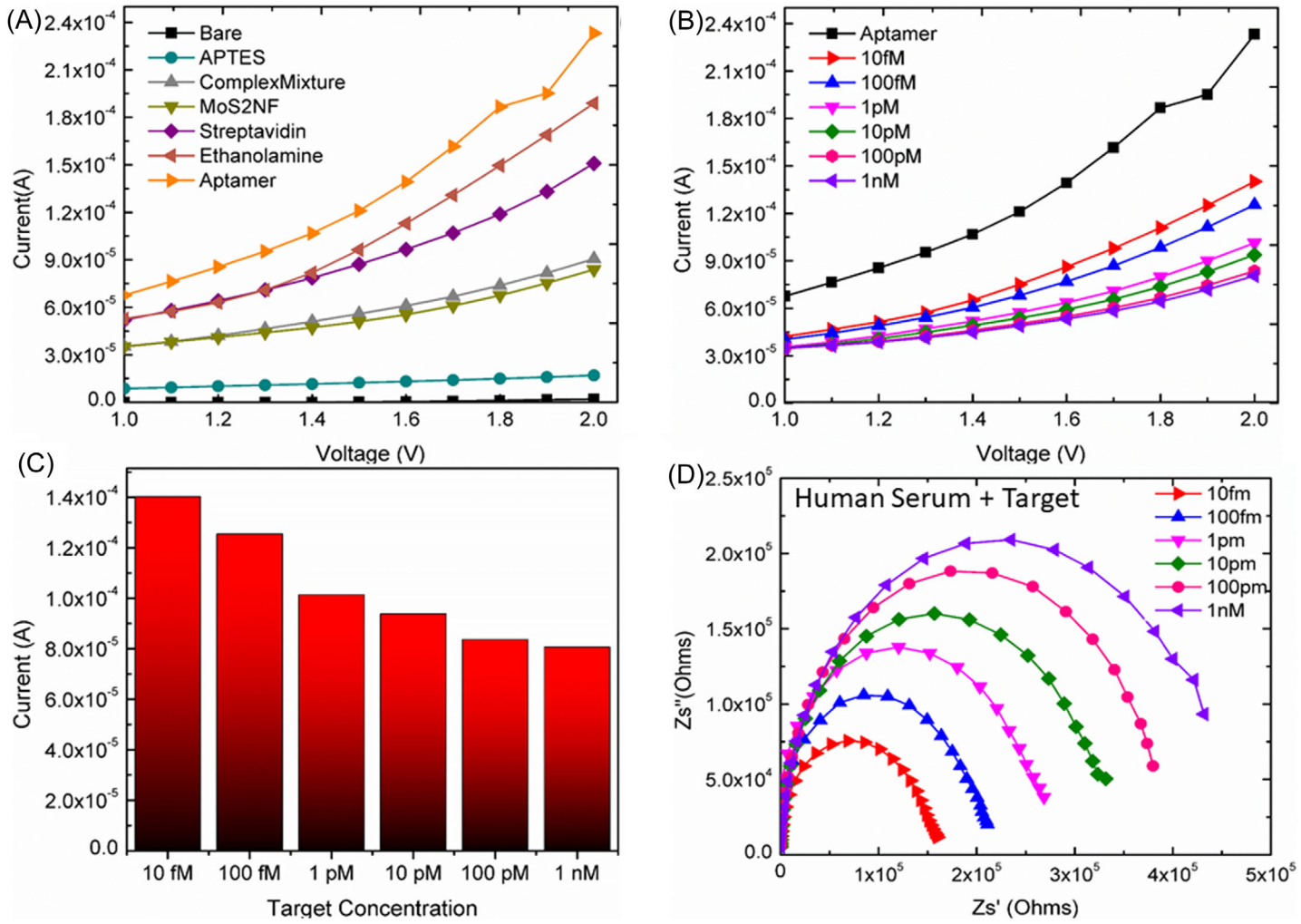

FIG. 5 *(A) Surface modifications on SPE electrode and (B) analysis of limit of detection using different concentrations of target (1 pM to 10 fM) through voltammetry measurements are shown. (C) A bar diagram to distinguish the current value of various target concentrations at 2 V. (D) Impedance spectra measurement to identify the selectivity of the biosensor. Human serum with the presence of other biomolecules is tested.*

respectively. Besides that, 10 and 100 pM corresponds to an Rct level of 3.3×10^5 and 3.8×10^5 Ω. The lowest detection limit for human serum is therefore 10 fM, similar to the detection limit in the absence of serum. The ability of the biosensor to detect troponin I in the presence of other proteins from human serum is remarkable, testimony to the high-performance nature of this biosensor.

3.9. Analytical performance of troponin I sensor

Figure 6A shows the linear regression analysis of the sensor sensitivity for various troponin I concentrations with $y = 2.4770\text{E}{-4} + 1.2293\text{E}{-5}\,X$ and $r^2 = 0.9919$. The sensitivity of the sensor was calculated using the following equation:

$$\text{Sensitivity} = \frac{\text{slope of calibration plot, m } (\mu\text{A mM}^{-1})}{\text{active surface area, A } (\text{cm}^2)}$$

The sensitivity is 0.000098 μA mM^{-1} cm^{-2} for a SPE electrode working surface area of 0.12566 cm^2 with a diameter of 4 mm. The detail sensitivity calculation was shown in Supplementary Information. For the aptamer-based SPE electrode to be selective, the biosensor must be able to detect troponin I in the presence of different proteins in the human serum. Figure 6B shows that the charge transfer resistance, Rct with immobilization, troponin T, and other protein were not significantly changed. There is slight increase in Rct value for the troponin I spiked sample, as there is specific binding of troponin I to aptamer, even though there is very little troponin I. Furthermore, the interaction with troponin I is impressive, due to the direct interaction with pure troponin I. Moreover, the charge transfer resistance displays a ~fivefold increase in selectivity by aptamer for pure troponin I compared with immobilization of troponin T and other proteins present in the human serum such as troponin C, albumin, fibrinogen, and

TABLE 1 *Comparison of the currently available detection of troponin I*

Method	*Strategy*	*Limit of detection*	*Reference*
Aptasensor	Aptamer-based detection	1.0 Pm	[32]
Immunosensor	FET-based biosensor	0.006 Nm	[6]
Aptasensor	A sandwich aptamer-based SPCE using chronoamperometry	1.0 pM	[5]
Aptasensor	Aptamer-based gold electrode	10 Pm	[2]
Immunosensor	Silicon nano wire biosensor	5 Pm	[33]
Aptasensor	Aptamer/ETNE/STVD/MoS_2_NF/CM/Aptes/SPE	10 fM	Ongoing

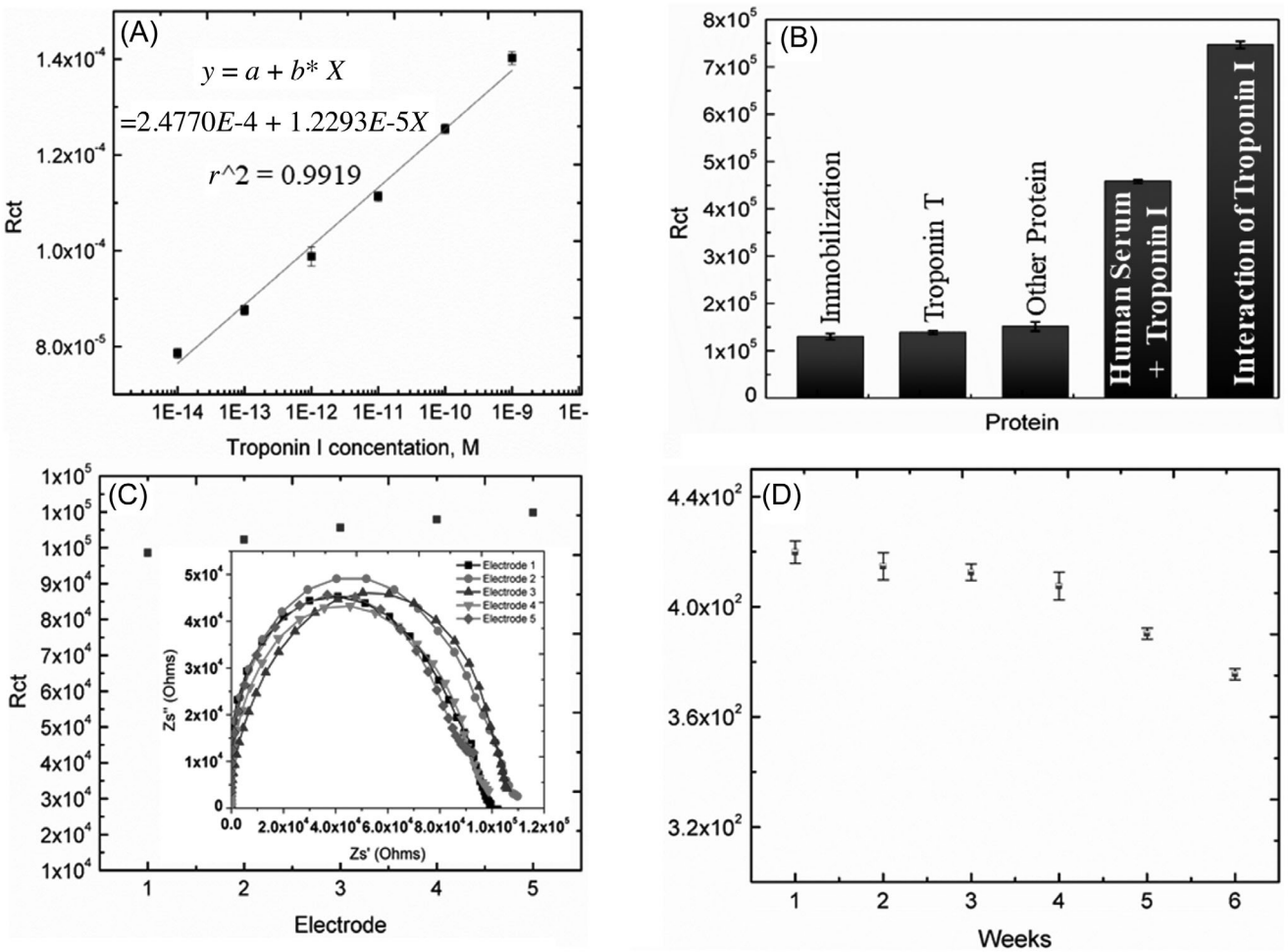

FIG. 6 *(A) Linear regression curve for different concentrations of target with a linear equation of ΔRct. (B) A bar diagram on selectivity of the biosensor and its Rct value. (c) Reproducibility of the biosensor using five different SPE electrodes. Inset graph is showing impedance spectra measurement of five electrodes. (D) Stability of the biosensor for past 6 weeks against Rct is shown.*

globulins. Specially designed aptamer does not capture these other proteins, as the aptamer only binds with troponin I. This biosensor therefore has excellent selectivity in the presence of other biomolecules in human serum. Besides that, the troponin I biosensor has good repeatability with a relative standard deviation (RSD) of 4.3% for five parallel devices prepared under the similar processing procedure, as shown in Fig. 6C. To validate the shelf-life of the electrode, stability checks were performed for each hybridized electrode for 6 weeks and stored at a temperature 4 °C. The stability analysis shows that the

sensor used in the current work is stable and exhibits a loss of only 10% of its activity after 6 weeks of time, as shown in Fig. 6D.

4. Conclusions

The unique characteristics of 3D flower-like MoS_2 enable the immobilization of aptamer for the detection of troponin I. The fabricated electrochemical biosensor is able to identify troponin I with high selectivity and sensitivity, where the selectivity was ~fivefold better than other proteins found in human serum, with 0.10 nA μM^{-1} cm^{-2} sensitivity. This sensor can detect the cTn1 biomarker at concentration as low as 10 fM and is stable for 42 days (at 4 °C). It is a promising alternative method for early AMI identification to provide a quick treatment for AMI diagnosed patients. This approach could potentially be expanded to act as a single platform for multiple detection strategies in the future.

5. Acknowledgements

The authors would like to thank Universiti Teknologi Petronas (UTP) for the financial support provided through URIF Grant (015LBO-021) and for the opportunity to conduct the research in the Nanotechnology Research Laboratory and Dye Solar Cell Laboratory. The authors also would like to thank Universiti Malaysia Perlis (UniMAP) for providing the facilities to conduct voltammetry experiment at Institute of Nano Electronic Engineering (INEE). N.J wants to acknowledge the Brazilian funding agencies: Sao Paulo Research Foundation – FAPESP (2014/23546-1, 2016/23474-6).

6. Author Contributions

M.V. synthesized and developed the MoS_2 nanostructures. M.V. and M.T. carried out the experiment and drafted the manuscript. S.C.B.G., S.S.M., N.M.M., N.J., and M.O. proof-read the manuscript. V.P. supervised the work. All authors analyzed the results and contributed to the discussion presented in the manuscript.

7. Additional Information

The authors declare no competing financial interests. During submission the supplementary information were attached together with this paper. Correspondence and requests for materials should be addressed to M.V. or V.P.

8. References

[1] Regan, B., O'Kennedy, R., and Collins, D. (2018) Biosensors 8, 1–32.
[2] Hospital, S., and Biosciences, H. (2018) J. Med. Investig. 53, 34–41.
[3] Zhang, B., Tamez-Vela, J. M., Solis, S., Bustamante, G., Peterson, R., Rahman, S., Morales, A., Tang, L., and Ye, J. Y. (2013) J. Med. Eng. 2013, 1–7.
[4] Yang, X., Zhao, Y., Sun, L., Qi, H., Gao, Q., and Zhang, C. (2018) Sens. Actuat. B Chem. 257, 60–67.
[5] Jo, H., Her, J., Lee, H., Shim, Y. B., and Ban, C. (2017) Talanta 165, 442–448.
[6] Sarangadharan, I., Regmi, A., Chen, Y. W., Hsu, C. P., chi Chen, P., Chang, W. H., Lee, G. Y., Chyi, J. I., Shiesh, S. C., Bin Lee, G., and Wang, Y. L. (2018) Biosens. Bioelectron. 100, 282–289.
[7] Tadepalli, S., Kuang, Z., Jiang, Q., Liu, K. K., Fisher, M. A., Morrissey, J. J., Kharasch, E. D., Slocik, J. M., Naik, R. R., and Singamaneni, S. (2015) Sci. Rep. 5, 1–11.
[8] Perumal, V., and Hashim, U. (2014) J. Appl. Biomed. 12, 1–15.
[9] Sharma, A., and Jang, J. (2019) Sci. Rep. 9, 1–10.
[10] Jun, J., Lee, J. S., Shin, D. H., and Jang, J. (2014) ACS Appl. Mater. Interfaces 6, 13859–13865.
[11] Zhu, X., Liang, X., Fan, X., and Su, X. (2017) RSC Adv. 7, 38119–38124.
[12] Veeramalai, C. P., Li, F., Liu, Y., Xu, Z., Guo, T., and Kim, T. W. (2016) Appl. Surf. Sci. 389, 1017–1022.
[13] Fan, X., Li, Z., Wang, S., Liu, L., Liu, P., Chen, F., and Zheng, X. (2019) J. Braz. Chem. Soc. 30, 1762–1768.
[14] Parra-Alfambra, A. M., Casero, E., Vázquez, L., Quintana, C., del Pozo, M., and Petit-Domínguez, M. D.(2018) Sens. Actuat. B Chem. 274, 310–317.
[15] Hu, S., Chen, W., Zhou, J., Yin, F., Uchaker, E., Zhang, Q., and Cao, G. (2014) J. Mater. Chem. A 2, 7862–7872.
[16] Lai, W., Chen, Z., Zhu, J., Yang, L., Zheng, J., Yi, X., and Fang, W., (2016) Nanoscale 8, 3823–3833.
[17] Vattikuti, S. V. P., and Byon, C. (2015) J. Nanomater. 2015. https://doi.org/10.1155/2015/710462.
[18] Liu, X., Xing, Z., Zhang, Y., Li, Z., Wu, X., Tan, S., Yu, X., Zhu, Q., and Zhou, W. (2017) Appl. Catal. B Environ. 201, 119–127.
[19] Hu, L., Ren, Y., Yang, H., and Xu, Q. (2014) ACS Appl. Mater. Interfaces 6, 14644–14652.
[20] Wang, D., Pan, Z., Wu, Z., Wang, Z., and Liu, Z. (2014) J. Power Sources 264, 229–234.
[21] Song, D., Wang, Y., Lu, X., Gao, Y., Li, Y., and Gao, F. (2018) Sens. Actuat. B Chem. 267, 5–13.
[22] Perumal, V., Hashim, U., Gopinath, S. C. B., Haarindraprasad, R., Foo, K. L., Balakrishnan, S. R., and Poopalan, P. (2015) Sci. Rep. 5, 1–12.
[23] Perumal, V., Hashim, U., Gopinath, S. C. B., Haarindraprasad, R., Poopalan, P., Liu, W. W., Ravichandran, M., Balakrishnan, S. R., and Ruslinda, A. R. (2016) Biosens. Bioelectron. 78, 14–22.
[24] Ma, N., Zhang, T., Fan, D., Kuang, X., Ali, A., Wu, D., and Wei, Q. (2019) Sens. Actuat. B Chem. 297, 126821.
[25] Wang, B., Zhong, X., Chai, Y., and Yuan, R. (2017) Sens. Actuat. B Chem. 245, 247–255.
[26] Yi, M., and Zhang, C. (2018) RSC Adv. 8, 9564–9573.
[27] Rheem, Y., Han, Y., Lee, K. H., Choi, S. M., and Myung, N. V. (2017) Nanotechnology 28. https://doi.org/10.1088/1361-6528/aa5c2f.
[28] Yan, J., Rath, A., Wang, H., Yu, S. H., Pennycook, S. J., and Chua, D. H. C. (2019) Mater. Res. Lett. 7, 275–281.
[29] Haarindraprasad, R., Hashim, U., Gopinath, S. C. B., Perumal, V., Liu, W. W., and Balakrishnan, S. R. (2016) Anal. Chim. Acta 925, 70–81.
[30] Gopinath, S. C. B., Perumal, V., Balakrishnan, S. R., Md Arshad, M. K., Lakshmipriya, T., Haarindraprasad, R., and Hashim, U. (2017) Microchim. Acta 184, 4425–4431.
[31] Lv, Q., Wang, Y., Su, C., Lakshmipriya, T., Gopinath, S. C. B., Pandian, K., Perumal, V., and Liu, Y. (2019) Int. J. Biol. Macromol. 134, 354–360.
[32] Jo, H., Gu, H., Jeon, W., Youn, H., Her, J., Kim, S. K., Lee, J., Shin, J. H., and Ban, C. (2015) Anal. Chem. 87, 9869–9875.
[33] Kim, K., Park, C., Kwon, D., Kim, D., Meyyappan, M., Jeon, S., and Lee, J. S. (2016) Biosens. Bioelectron. 77, 695–701.